RSC Advances

PAPER

View Article Online
View Journal | View Issue

Cite this: *RSC Adv.*, 2026, **16**, 29688

Self-absorption correction in calibration-free laser-induced breakdown spectroscopy for quantitative elemental profiling and chemometric classification of *Spinacia oleracea*

Ambreen Aslam, *[a] Abdul Ghuffar[a] and Zahid Farooq[b]

Although Laser-Induced Breakdown Spectroscopy (LIBS) is a fast multi-elemental technique, with increasing applications in agricultural diagnostics, self-absorption can affect its quantitative sensitivity. In the present work, Calibration Free LIBS (CF-LIBS) of healthy and diseased spinach leaves was combined with Internal Reference Self Absorption Correction (IRSAC) to enhance the consistency of the spectral results to profile the elements. Leaf spot infection is known to interfere with ionic transport and chlorophyll metabolism, leading to variations in macronutrients (Ca, Mg, and K) and micronutrients (Fe, Mn). Accordingly, corrected LIBS emissions were used to evaluate physiologically relevant trends. Plasma temperature and electron density were determined using Boltzmann plots and Stark broadening to verify local thermodynamic equilibrium (LTE) conditions. To establish quantitative reliability, CF-LIBS concentrations were cross-validated against inductively coupled plasma optical emission spectroscopy (ICP-OES), yielding deviations within 7–10%, consistent with values reported in established LIBS validation studies. Multivariate analysis using principal component analysis (PCA) demonstrated clear clustering between healthy and diseased samples, while supervised machine learning (ML) classifiers achieved >90% accuracy. The integrated IRSAC corrected CF-LIBS and ML framework demonstrates the potential of spectroscopically validated elemental profiling and may support further development of portable systems for precision agriculture and food-quality monitoring.

Received 5th March 2026
Accepted 27th May 2026

DOI: 10.1039/d6ra01889k

rsc.li/rsc-advances

1. Introduction

Laser-Induced Breakdown Spectroscopy (LIBS) has a severe drawback known as self-absorption effect, in which strong emission lines are reabsorbed in the plasma. This distortion changes the spectral intensities, which results in the imprecision of quantifying elemental concentrations and unreliable plasma diagnostics.[1] This is a critical issue of concern to the reliability of LIBS, especially in agricultural and biological research where minor compositional variations between healthy and diseased tissues need to be resolved. The Internal Reference Self-Absorption Correction (IRSAC) method is one of the existing strategies that has proven to be significant in restoring the actual line intensities and enhancing the accuracy of analysis.[2] A good example of application in this regard is crop health monitoring. The conventional methods of analysis, such as Atomic Absorption Spectroscopy (AAS) and Inductively Coupled Plasma Optical Emission Spectroscopy (ICP-OES), have been found to be useful in the analysis of nutrients and contaminants, but are destructive, demand a lengthy preparation time, and are only applicable to the laboratory environment, which limits their use in rapid or field-based diagnostics.[3] Comparatively, LIBS can deliver multiple elements in real-time, *in situ*, and with minimum sample preparation, and this is why it may be applied in agriculture.[4]

Leafy vegetables, such as spinach (*Spinacia oleracea*) which are nutritionally important are very vulnerable to biotic and abiotic stresses such as nutrient deficiencies, pollution and pathogenic infections.[5] Foliar diseases like leaf spots do not only reduce yield and market quality but also alter tissue composition which is harmful to food safety and consumer health. Correct and timely identification of such physiological and pathological alterations is thus paramount and self-absorption-corrected LIBS method is a route to proper elemental profiling and successful disease surveillance in spinach farming. Simultaneously, recent developments in the field of the data-driven models have demonstrated that chemometric and machine learning algorithms can be used effectively to classify the plant health conditions based on complicated spectral data sets.[6–10] PCA may be used to reduce the dimensions and visualize the variance, whereas supervised

[a]*Department of Physics, Riphah International University, Faisalabad Campus, Faisalabad, Pakistan. E-mail: ambreen1153@gmail.com*
[b]*Department of Physics, Division of Science and Technology, University of Education, Lahore, Pakistan*

algorithms, including Support Vector Machines (SVM), Random Forests (RF) and *k*-Nearest Neighbors (kNN) are widely used in disease identification and crop monitoring.[11–13] Although LIBS and machine learning have been independently studied in the context of plant health diagnostics, calibration-free IRSAC has been studied in different applications, no research has been carried out to systematically integrate IRSAC-corrected LIBS with machine learning to detect spinach health status.

Even though LIBS and machine learning have been explored in the past to measure plant-health, all the existing literature must either use uncorrected spectra or external calibration, or qualitative classification without accounting for self-absorption and matrix-related distortions. The current research makes three important contributions. To obtain physically meaningful intensities with reliable CF-LIBS quantification, First, Internal Reference Self-Absorption Correction (IRSAC) was introduced that provides a systematic correction of line-profile distortion and recovers physically meaningful intensities. Second, the fixed spectrums are checked with ICP-OES using nutritionally relevant macro and micronutrients (Ca, Mg, K, Fe, Mn), showing the deviation to less than 10% and confirming that IRSAC assisted CF-LIBS is credible in the analysis of leaf elementals. Third, it combines the fixed quantitative characteristics into an ML pipeline of healthy and diseased spinach into a spectroscopically corrected plasma diagnostics and quantitative chemistry model and machine-learning-based classifier within a system. Such an approach bridges a serious gap in the literature as it shows that self-absorption corrected LIBS intensities are much more useful in quantitative elemental analysis and classification reliability.

2. Materials and methods

Two types of *Spinacia oleracea* were studied, the samples were taken in fields of agriculture in Faisalabad, Pakistan: healthy leaves without obvious symptoms and diseased leaves with clear symptoms of leaf spots. Here, spinach leaves that display early to moderate symptoms of leaf spot disease, a prevalent fungal-bacterial stresses disease in leafy greens, were chosen to provide biological meaningful comparison of the healthy and diseased tissue.[14] After collecting, samples were washed with double distilled water to remove the stuck dust and soil particles, dried at ambient conditions and subsequently dried in vacuum oven at 60 °C conditions, over a duration of 2 h of time.[15] Leaves were dried and crushed to fine powder in a specially designed ball mill and finally sieved.[16] Each fraction (approximately 500 mg) was squeezed into circular pellets (13 mm diameter, or about 2 mm thickness) under 10 tons of pressure with a hydraulic press. These pellets were taken as LIBS targets.[17] ICP-OES samples were prepared using the normal wet-acid digestion in HNO_3 and then dilution and filtration followed.[3]

The second harmonic (532 nm) of a Q-switched Nd:YAG laser (Q-Smart 850) was used to generate plasma on the surface of the spinach pellets. The laser delivered pulses of 5 ns duration with an energy of approximately 103 mJ per pulse. The beam was focused onto the sample surface using a 10 cm focal-length lens. To reduce crater formation and improve representative ablation, the pellets were mounted on a rotating holder so that a fresh surface was exposed to each laser pulse.[18] The plasma emission was collected in an orthogonal geometry using a lens–fiber assembly and transferred to an Avantes echelle spectrograph equipped with a CCD detector, as shown in Fig. 1. The

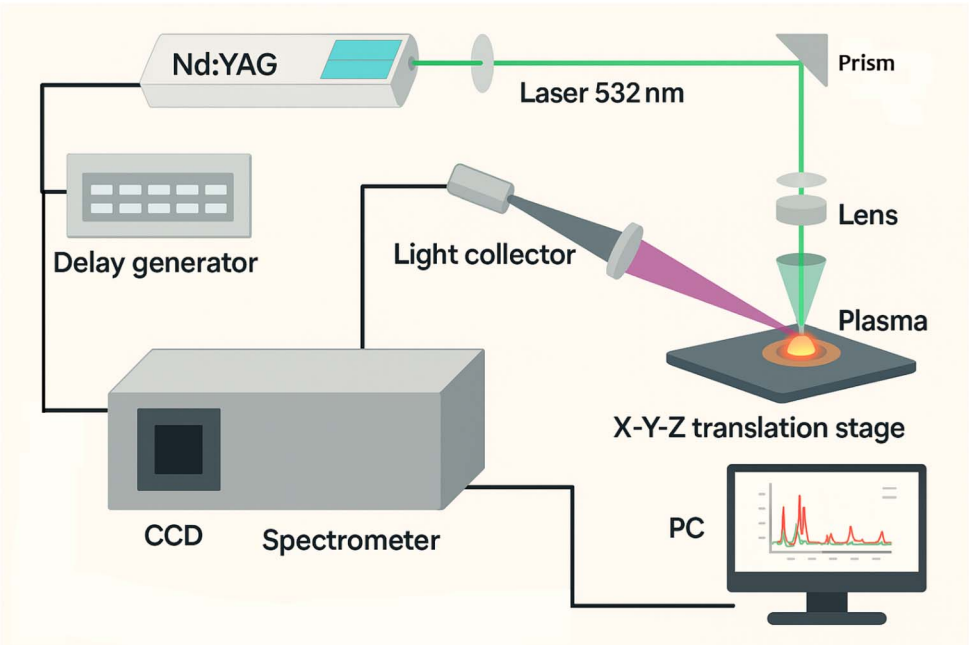

Fig. 1 Schematic of the LIBS experimental setup showing laser irradiation of spinach pellets and optical emission collection into the spectrometer.

spectrometer covered the 190–770 nm range in a single acquisition, with a wavelength resolution of approximately 0.03–0.08 nm. Spectral acquisition and visualization were controlled using AvaSoft 8.5 software. The acquisition parameters were selected to maximize the signal-to-noise ratio and reduce continuum background, with a gate delay of 1 μs and a gate width of 10 μs per shot.[19,20] Five pellets were prepared for each sample type, healthy and diseased, and 20 spectra were recorded from each pellet.

All recorded spectra were first corrected for the dark-current background acquired with the laser blocked, using the Avantes AvaSoft routine. The continuum baseline was then removed using an asymmetric least-squares (AsLS) algorithm with smoothness parameter $\lambda = 10^5$ and asymmetry parameter $p = 0.001$, implemented in Python (SciPy). A Savitzky–Golay filter with a 7-point window and third-order polynomial was applied for noise smoothing before peak detection. Peaks were located using the prominence-based local-maximum routine find_peaks in SciPy v1.13, with prominence and width thresholds checked against the NIST Atomic Spectra Database within a ±0.07 nm tolerance. Each detected line was fitted with a Lorentzian profile to extract the line-centre wavelength, peak intensity, and FWHM.[21–23]

All healthy and diseased spinach spectra were acquired under identical optical geometry, spectrometer settings, gate delay, gate width and laser energy; therefore, the comparative spectral analysis was performed under internally consistent instrumental conditions. The optical-thinness checks used closely spaced resonance doublets, *e.g.* Mg II 279.553/280.270 nm, for which detector-response variation across each pair is expected to be minimal. The IRSAC-corrected CF-LIBS concentrations were further cross-verified against ICP-OES for Ca, Mg, K, Fe and Mn to evaluate quantitative consistency. Future work may further improve absolute quantification by applying full radiometric response calibration over the 190–770 nm range.

IRSAC correction factors and CF-LIBS quantification were derived from pellet-averaged spectra to improve signal-to-noise ratio, while PCA and machine-learning classification were performed on individual shot spectra after applying the corresponding pellet-specific IRSAC correction factors.[24] The emission lines were post-acquisition matched to the NIST Atomic Spectra Database within ±0.07 nm and categorized into macro-, micro- and trace/toxic-element groups to form sample-wise elemental profiles.[25] Plasma temperature and electron density were determined using Boltzmann plots and Stark broadening of isolated lines, respectively. LTE validity was evaluated using the McWhirter criterion, and IRSAC was applied before recalculating plasma parameters and concentrations to reduce reabsorption-related artifacts and improve quantitative consistency.[26–30] The workflow of the present work is shown in Fig. 2.

Principal Component Analysis (PCA) was initially used to perform dimensionality reduction of LIBS spectra to emphasize the difference between healthy and diseased spinach samples.[31] To be classified, random forest (RF), *k*-Nearest Neighbours (kNN), and Support Vector Machines (SVM) supervised machine learning algorithms were applied.[32,33] The chemometric and classification analyses were done in MATLAB R2025a (MathWorks, Natick, USA) Classification Learner Toolbox and Python 3.11 (scikit-learn v1.5.0, NumPy, pandas, and matplotlib libraries). To ensure strict biological independence and prevent shot-level data leakage, model performance was evaluated using Leave-One-Group-Out (LOGO) cross validation (Fig. 3), where all

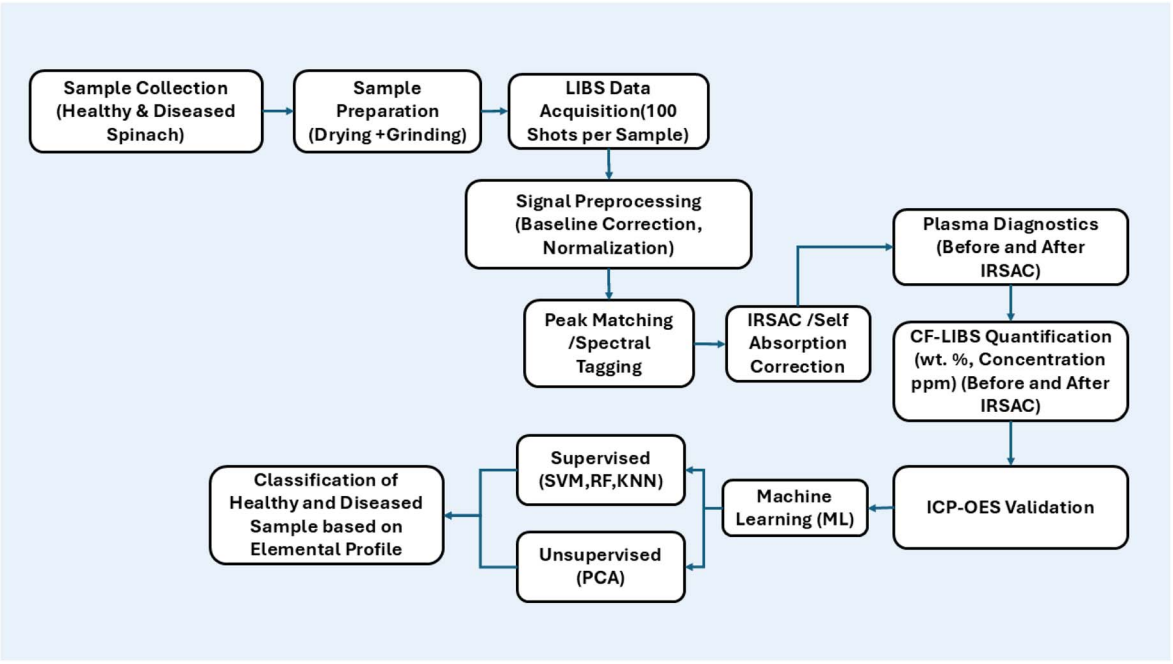

Fig. 2 Workflow of the IRSAC-corrected CF-LIBS methodology applied for healthy and diseased spinach analysis.

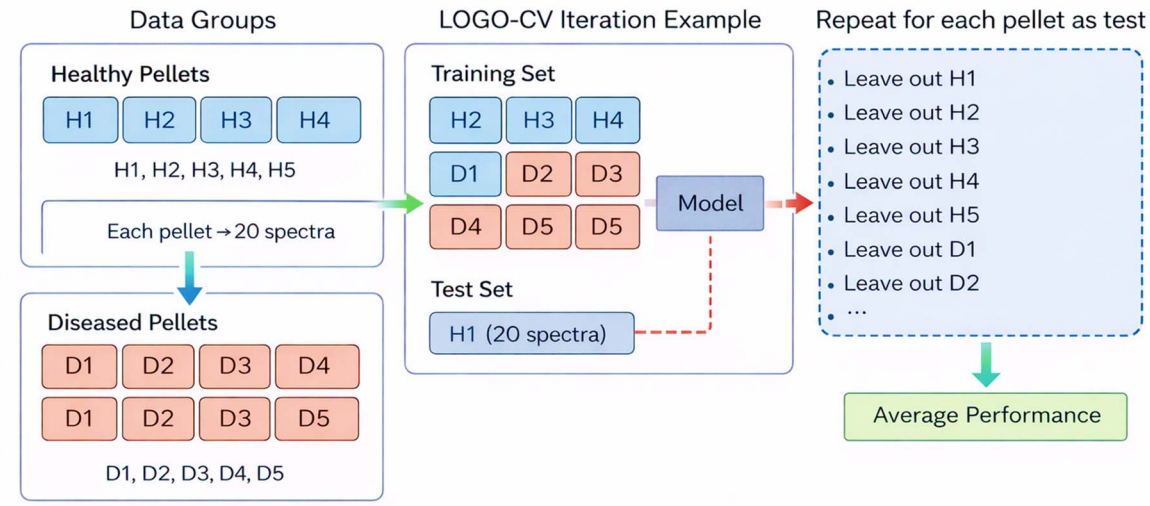

Fig. 3 Schematic of the Leave-One-Group-Out (LOGO) cross validation strategy.

spectra from one pellet were excluded from training and used exclusively for testing in each fold. The performance metrics were confusion matrices, accuracy, and area under ROC curves (AUC).[34,35]

3. Results and discussion

3.1 Spectral characteristics and elemental features

The spectral interpretation of the LIBS data began with pre-processing of the recorded data to increase the reliability of the signal and to reduce other artifacts that were due to the matrix.[36] The processes involved in the workflow were baseline subtraction, peak detection, and estimation of the FWHM. Peaks in the spectrum were then determined automatically by finding local peaks that passed by a prominent criterion. The entire width at half maximum (FWHM) (eqn (1)) of detected lines was determined as shown by:

$$\mathrm{FWHM} = \Delta\lambda \times n_{1/2} \quad (1)$$

where $\Delta\lambda$ is the local channel spacing in nm/pixel (extracted from the spectrometer's native wavelength array) and $n_{1/2}$ is the number of pixels above half-maximum. This relation provides only an initial FWHM estimate; the value used in all subsequent analysis was taken from a Lorentzian fit to the same line. The stacked LIBS spectra of healthy and diseased sample spinach fall under the range of 190–770 nm as illustrated in Fig. 4. The most significant emission lines were attributed to the macro-nutrients like Ca II (393.36, 396.85 nm), Mg II (279.55 and 280.27 nm) and the Na I doublet (588.99, 589.59 nm). There were also some lines of micronutrient, such as Fe I (407.17, 407.61, 500.20 nm), Zn I(462.98, 468.01 nm) and Mn I (279.83 nm). Moreover, trace and possibly toxic elements were detected (Pb I 368.96, 368.35 nm), Hg II (391.92 nm), Cr I (425.43, 427.48, 428.97, 430.11, 520.45 nm), Al I (396.15 nm), Al II (399.58 nm) and Cd I (508.58 nm). Only the most prominent and analytically relevant lines are labelled for clarity; additional matched lines, including Hg, V, P, Ag Ti, Ni and Pb, are listed in the supplementary line-assignment table. The Ca II, Mg II, Fe I and K lines represented nutrient sufficiency in healthy spinach spectra and suppressed signals of Mg, Ca, K and Mn in diseased spinach, which are essential in photosynthetic and enzymatic activities.[37,38] Conversely, trace elements like Pb, Hg and Cd showed a relatively high emission in disease samples connoting that uptake and accumulation of these elements changed when one became diseased. Spectra of diseased also exhibited slightly broader and less sharp peaks, which were associated with plasma-matrix effects, which are related to biochemical changes. These spectral intensity changes in macro, micro and trace element lines form the basis of the further plasma diagnostics and chemometric classification. Even before applying multivariate analysis, the spectra themselves reveal clear elemental differences between healthy and diseased spinach, underscoring the discriminative capability of LIBS for plant health monitoring.[39–41]

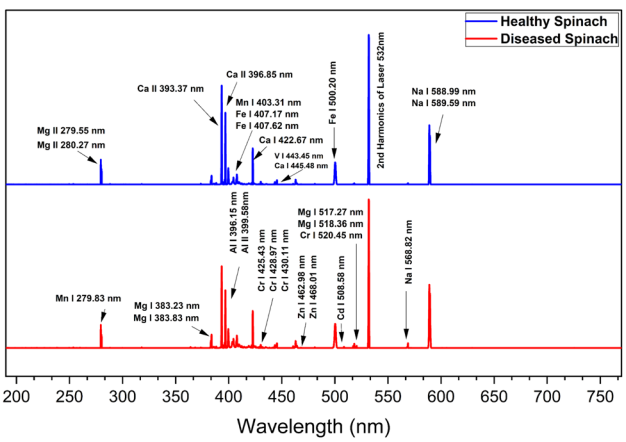

Fig. 4 Representative LIBS spectra of healthy and diseased spinach samples, vertically offset for clarity.

3.2 Plasma diagnostics before and after IRSAC

The plasma excitation temperature was estimated using the Boltzmann plot method, which relies on the assumption of local thermodynamic equilibrium (LTE). According to this method, the intensity I_{ij} of an emission line from an upper energy level j to a lower level i is given by eqn (2):

$$I_{ij} = \frac{hc}{4\pi}\frac{A_{ji}g_j}{U(T)}N\lambda\exp\left(-\frac{E_j}{k_B T}\right) \quad (2)$$

where (A_{ji}) is the transition probability,(g_j) is the statistical weight of upper level,(E_j) is the upper energy level in eV, (λ) is the transition wavelength, $(U(T))$ is the partition function, (N) is the total number density, (T) is the plasma excitation temperature in Kelvin, (k_B) is the Boltzman's constant, (h) is the Planck's constant and (c) is the speed of light. By taking the natural logarithm and rearranging, the linearized form is:

$$\ln\left(\frac{I_{ij}\lambda}{A_{ji}g_j}\right) = -\frac{E_j}{k_B T} + \text{constant} \quad (3)$$

Plotting $\left(\ln\left(\frac{I_{ij}\lambda}{A_{ji}g_j}\right)\right)$ *vs.* (E_j) yields a straight line whose slope is $\left(-\frac{1}{k_B T}\right)$, from this slope the plasma excitation temperature can be calculated. In the study, Boltzmann plots were constructed for selected neutral and singly ionized calcium (Ca II) lines in healthy and diseased spinach plasmas. The estimated plasma temperatures obtained from the Boltzmann plots were 7598 K for healthy spinach and 6859 K for diseased spinach, as shown in Fig. 5(a) and (b). Weak plasma excitation in diseased spinach plasma indicates low excitation temperature, which could be caused by changes in the elemental composition and the levels of the essential nutrients like calcium (Ca), potassium (K), and magnesium (Mg).[42] These temperature estimates justify the selection of emission lines to be diagnostic and give the needed input to further calculations, such as electron density accurate determination, and self-absorption remediation. In Table 1, the spectroscopic parameters (wavelengths, transition probabilities, upper and lower energy levels and statistical weights) of the chosen Ca II transitions are listed.

The electron density N_e of the plasma was calculated using the Stark broadening method (eqn (4)), which exploits the dependence of spectral line broadening on plasma electron density.[43] For an isolated spectral line, the Stark broadening relation can be expressed as:

$$\Delta\lambda_{\text{measured}} = \Delta\lambda_{\text{Stark}} \approx 2w\left(\frac{N_e}{10^{16}}\right) \quad (4)$$

where $\Delta\lambda_{\text{measured}}$ is the experimentally measured full width at half maximum (FWHM), w is the electron impact parameter obtained from reference Stark tables, and N_e is the electron density (cm^{-3}).[44] As shown in Fig. 5(c), a Lorentz fit to the Ca II 393.366 nm line (healthy: red; diseased: black) provided the Stark FWHM used to compute N_e. For the present study, the Ca II line at 393.366 nm was selected due to its well-documented Stark parameters and high sensitivity to plasma electron density.[45] The validity of local thermodynamic equilibrium (LTE) was further confirmed using the McWhirter criterion given in eqn (5):[29]

$$N_e \geq 1.6 \times 10^{12} T^{1/2}(\Delta E)^3 \quad (5)$$

where T is the plasma temperature in Kelvin and ΔE is the largest energy gap (in eV) between the upper and lower states considered in the Boltzmann plot. For the estimation of electron number density, the Stark broadening of the Ca II line at 393.366 nm was employed as the diagnostic line given in Table 1. In particular, the transition at 393.366 nm served as the reference for evaluating Stark broadening and deriving the corresponding electron density values. For healthy spinach plasma, the measured FWHM was 0.2397 nm, yielding an estimated electron density of $(8.38 \pm 0.01) \times 10^{17}$ cm^{-3}. The McWhirter minimum density was calculated as $(8.44 \pm 0.01) \times 10^{15}$ cm^{-3}, confirming LTE validity. For diseased spinach plasma, the measured FWHM was slightly lower (0.2366 nm), corresponding to an electron density of $(8.27 \pm 0.01) \times 10^{17}$ cm^{-3}. The McWhirter criterion gave a threshold of $(8.02 \pm 0.01) \times 10^{15}$ cm^{-3}, again confirming LTE.

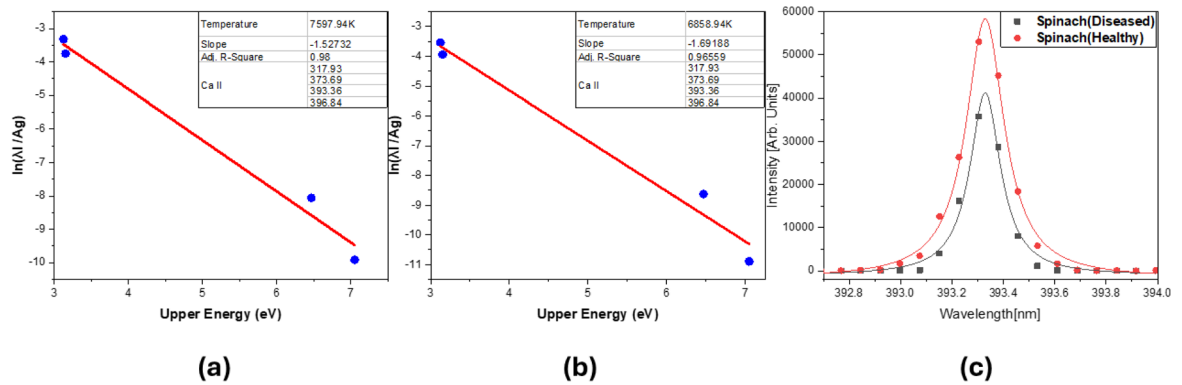

Fig. 5 (a) Boltzmann plot for excitation temperature of healthy and (b) diseased spinach samples (c) Lorentzian fit of Ca II 393.36 nm line for healthy and diseased spinach samples.

Table 1 Spectroscopic data of Ca II transitions used for Boltzmann plot

Line	Wavelength (nm)	Transition probability $A \times 10^7$ (s^{-1})	Lower energy E (eV)	Upper energy E_k (eV)	g	g_k	Transition
Ca II	317.933	36.0	3.150984	7.049551	4	6	$3p^6 4d \rightarrow 3p^6 4p$
Ca II	373.690	17.0	3.150984	6.467875	4	2	$3p^6 5s \rightarrow 3p^6 4p$
Ca II	393.366	14.7	0.000000	3.150984	2	4	$3p^6 4p \rightarrow 3p^6 4s$
Ca II	396.847	14.0	0.000000	3.123349	2	2	$3p^6 4p \rightarrow 3p^6 4s$

3.3 IRSAC influence on line intensities and element profiles

Although the values of the baseline plasma temperature and electron density are physically sound, the measured distribution in Boltzmann plots and distortions in the Lorentzian fits emphasize the weakness of the raw self-absorbed spectra.[24] The intensities of alkali elements such as Na and K were also abnormally high instead of expected trends and this is a characteristic of self-absorption that is quite familiar.[46] These are effects that may bias quantitative elemental analysis as well as plasma diagnostics unless mitigated.[47] To reduce the effect of self-absorption on the recorded emission line intensities, the Internal Reference Self-Absorption Correction (IRSAC) technique was used.[48] The IRSAC methodology is based on the choice of an optically thin transition in each element-ion group as an internal reference line, which is referred to as I_{ref}. The reference was usually selected as one of transitions having high excitation energy (E_{ref}) and comparatively small transition probability (A_{ref}) to minimize the possibility of self-absorption effects. The formulation of the IRSAC method is presented by the eqn (6).

$$f_k = \frac{I_k A_{ref} g_{ref}}{I_{ref} A_k g_k} \exp\left(- \frac{E_{ref} - E_k}{k_B T} \right) \quad (6)$$

with I_k the measured raw intensity of line k, A_k the Einstein transition probability, g_k the statistical weight of the upper level, E_k the excitation energy of the transition, k_B the Boltzmann constant and T the plasma temperature, which in this experiment was 7597.94 K in healthy and 6858.95 K in diseased spinach. In this approach, the correction is not applied as a single global scaling factor to the whole spectrum; rather, each emission line is corrected individually using a line-specific, wavelength-dependent correction factor. IRSAC was applied to the peak intensity obtained from the fitted Lorentzian profile of each selected transition. Therefore, each line k receives its own correction factor f_k, calculated from the corresponding spectroscopic parameters A_k, g_k, and E_k, relative to the selected internal reference line of the same species and ionization state. The IRSAC methodology is based on the choice of a minimally self-absorbed transition in each element-ion group as an internal reference line, referred to as I_{ref}. The reference line was selected from transitions having relatively high excitation energy (E_{ref}) and comparatively small transition probability (A_{ref}), where possible, to reduce the probability of strong self-absorption effects. The intensity of the line with the correction is then provided by:

$$I_{k,corr} = \frac{I_k}{f_k} \quad (7)$$

To evaluate line-profile distortion associated with self-absorption, representative Na I 588.99/589.59 nm, Mg II 279.553 nm, and Ca II 393.366 nm lines were examined using Lorentzian fitting (SI Table S3 and Fig. S2). The Na I resonance doublet showed the strongest broadening/central distortion, whereas Mg II 279.553 nm remained comparatively symmetric and narrow. The Ca II 393.366 nm line showed moderate broadening, the FWHM values were used only as diagnostic indicators of self-absorption related line profile distortion; IRSAC was applied to the analytical peak intensities used for CF-LIBS quantification, not as a physical reconstruction of the measured linewidth. It is important to clarify that the IRSAC approach applied in the present work is an analytical peak-intensity correction method rather than full physical reconstruction or deconvolution of the emission-line profile. Thus, IRSAC corrects the selected line intensities used for CF-LIBS quantification, but it does not explicitly resolve the wavelength-dependent optical thickness across the complete Lorentzian or Voigt emission profile. Advanced line-profile modelling frameworks, including τ-algorithm-based approaches and full Lorentz/Voigt profile treatments, can directly model optical-thickness effects across the line shape and therefore provide a more detailed description of self-absorption in laser-induced plasmas. These approaches are complementary to the present IRSAC-assisted CF-LIBS workflow and represent a useful direction for future refinement.[49,50] For an optically thin plasma, the ratio of two emission lines of the same ionic species and resonance doublet is fixed by atomic constants alone:

$$R_{th} = \frac{g_1 A_1 \lambda_2}{g_2 A_2 \lambda_1} \quad (8)$$

The Mg II 279.553/280.270 nm doublet gave a theoretical optically thin ratio of $R_{th} \approx 2.03$. The measured ratios were 1.95 for healthy spinach and 1.94 for diseased spinach, with deviations of ~4.0% and ~4.5%, respectively, supporting its use as a near optically thin reference pair. Although the IRSAC reference lines were chosen on the basis of practical low self-absorption criteria (high upper level energy, comparatively low transition probability, isolated and symmetric Lorentzian profile, and consistency in the Boltzmann plot) following Sun and Yu[51] and following the SAF-LIBS line selection approach

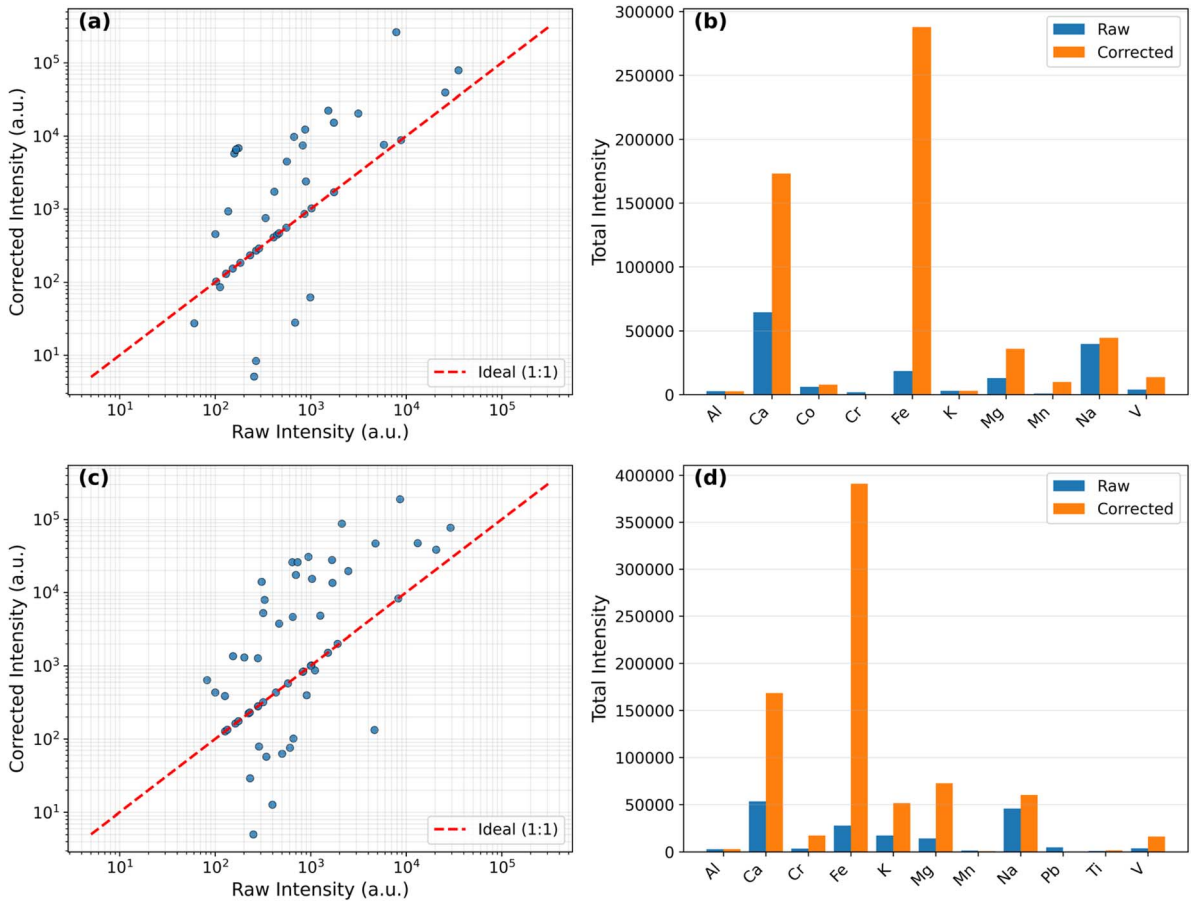

Fig. 6 Effect of IRSAC on LIBS emission intensities of spinach samples. (a) Healthy spinach: log–log plot of raw *vs.* corrected intensities, (b) corresponding bar graph showing enhanced Fe, Ca, and K signals. (c) Diseased spinach: similar trend with (d) increased corrected intensities bar plot.

reported by Hou *et al.*,[52] the near optically thin behavior of the selected reference lines was evaluated experimentally using the well-known doublet intensity ratio test.

The IRSAC correction results of healthy spinach are shown in Fig. 6(a) and (b) and diseased spinach is shown in Fig. 6(c) and (d). The log–log scatter plots of corrected and raw intensities in both instances show a shift to the desired 1 : 1 line (dashed red), and the bar graphs adjacent to them show that the total intensities of elements like Fe, Ca, and K improve considerably after correction. These results support the effectiveness of IRSAC in reducing self-absorption-related intensity bias while preserving the relative behavior of near-optically-thin transitions.[53]

The initial plasma temperature was estimated from a Boltzmann plot using four Ca II lines at 317.933, 373.690, 393.366, and 396.847 nm. This temperature was used as the starting input for IRSAC, consistent with the practical internal-reference self-absorption correction framework, in which an initial plasma temperature and selected internal reference line are used to calculate line-specific correction factors.[51,54] After applying IRSAC to the selected peak intensities, a second Boltzmann plot was constructed from the corrected intensities, giving updated diagnostic temperatures of 8164 K and 7062 K for healthy and diseased spinach, respectively, as shown in Fig. 7 and Table 2. The moderate changes from the initial values, approximately 7.5% and 3.0%, indicate improved Boltzmann-plot consistency while maintaining stable temperature correction.

To quantify the influence of self-absorption correction on each element, eqn (9) was used, an element-wise ratio was calculated as:

$$R_i = \frac{C_{i,\mathrm{IRSAC}}}{C_{i,\mathrm{SA}}} \tag{9}$$

where, $C_{i,\mathrm{IRSAC}}$ and $C_{i,\mathrm{SA}}$ are the IRSAC corrected and self-absorbed coefficients of the element i, respectively. When the ratio is greater than unity it depends on the fact that the elemental intensity has been underestimated by the self-absorbed spectrum, and when the ratio is lower than unity then it is the elemental intensity that has been overestimated. There were significantly higher ratios of diseased spinach compared to non-diseased spinach of macronutrients including K and Ca (ratio exceeding 3); thus, showing that these lines were highly repressed by self-absorption and recovered successfully after correction (Fig. 8). Na on the other hand had ratios of less than 1 in both healthy and diseased samples, suggesting

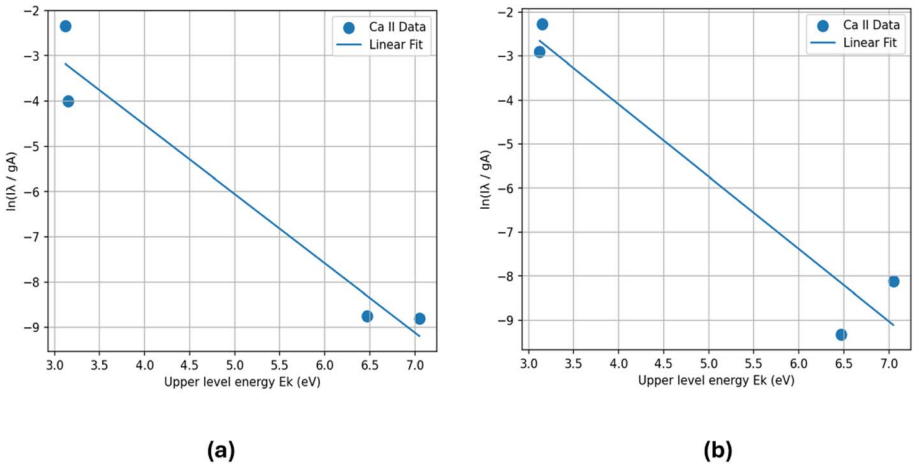

Fig. 7 Boltzmann plot after IRSAC correction (a) healthy spinach (b) diseased spinach.

Table 2 Plasma excitation temperature (T) and electron density (N_e) of spinach plasma before and after IRSAC correction

Sample	Plasma temp. before IRSAC (K)	Plasma temp. after IRSAC (K)	Electron density before IRSAC ($\times 10^{17}$ cm^{-3})	Electron density after IRSAC ($\times 10^{17}$ cm^{-3})
Healthy	7598	8164	8.38	8.45
Diseased	6859	7062	8.27	8.44

systematic overestimation in the self-absorbed spectrum. Many of the micronutrients like Fe and Ni had ratios near unity meaning that correction was minimal, whereas many of the toxic elements like Hg and Cd displayed higher ratios (>1) especially in diseased leaves, which is more easily detectable by IRSAC.[55,56] These findings point to the fact that IRSAC correction is not uniformly scaling but an element-specific adjustment hence producing an improved representation of the spinach elemental profile.

3.4 Quantitative CF-LIBS analysis

The elemental concentrations (weight%) of healthy and diseased spinach samples were determined using the calibration-free LIBS (CF-LIBS) approach combined with Internal Reference Self-Absorption Correction (IRSAC).[57] In this method, the measured intensity of each emission line was first corrected for self-absorption under internally consistent instrumental conditions and then used to calculate relative elemental abundances according to the CF-LIBS formalism.[58] Plasma temperature and electron density were derived from the Boltzmann plot and Stark broadening method, respectively, and incorporated into the concentration evaluation.

For each emission line, the elemental contribution was initially estimated as:[59]

$$C_{ij} = \frac{I_{ij} Z}{A_{ij} g_j} \exp\left(\frac{E_j}{k_B T}\right) \quad (10)$$

where I_{ij} is the self-absorption-corrected line intensity, A_{ij} the Einstein transition probability, the statistical weight of the upper level g_j, E_j the upper-level energy, T the plasma temperature, and Z the partition function of the species.

To account for both neutral and ionized species, the Saha–Boltzmann relation was applied:

$$\frac{n_e C^{z+1}}{C^z} = \left(\frac{2\pi m_e k_B T}{h^2}\right)^{3/2} \frac{U^{z+1}(T)}{U^z(T)} \exp\left(-\frac{E_{ion}}{k_B T}\right) \quad (11)$$

where C^z and C^{z+1} are the concentrations of neutral and ionized atoms, n_e is the electron density, E_{ion} is the ionization potential, and $U^z(T)$, $U^{z+1}(T)$ are the respective partition functions. The total elemental concentration was then obtained as:

$$C_i = \sum_{j \in i} C_{ij} = C^z + C^{z+1} \quad (12)$$

The relative abundance of each element was normalized with respect to the total contribution of all detected elements:

$$C_i^{rel} = \frac{C_i}{\sum_k C_k} \quad (13)$$

and expressed as weight percentage:

$$w_i = 100 \times C_i^{rel} \quad (14)$$

The procedure adopted is based on the CF-LIBS methodology.[57,58] Fig. 9 shows the comparative elemental distribution of healthy and diseased spinach samples in percentages of normalized weights. The logarithmic scale highlights both major and trace elements in many orders of magnitude. Ca, Fe, and Mg were also present in both sample groups, which is also

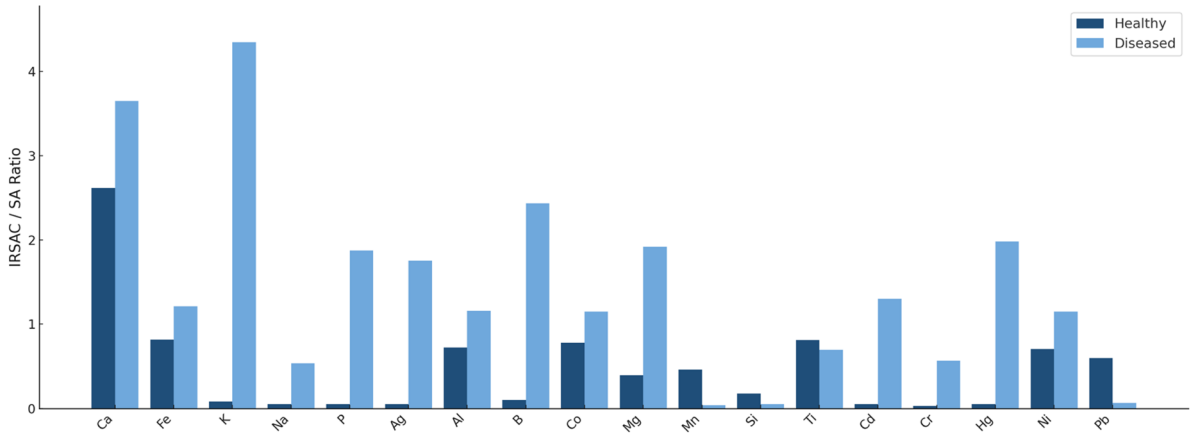

Fig. 8 IRSAC-to-SA ratios for spinach samples. Bars represent the ratio of IRSAC-corrected to self-absorbed coefficients (IRSAC/SA) for each element in healthy spinach (blue) and diseased spinach (orange).

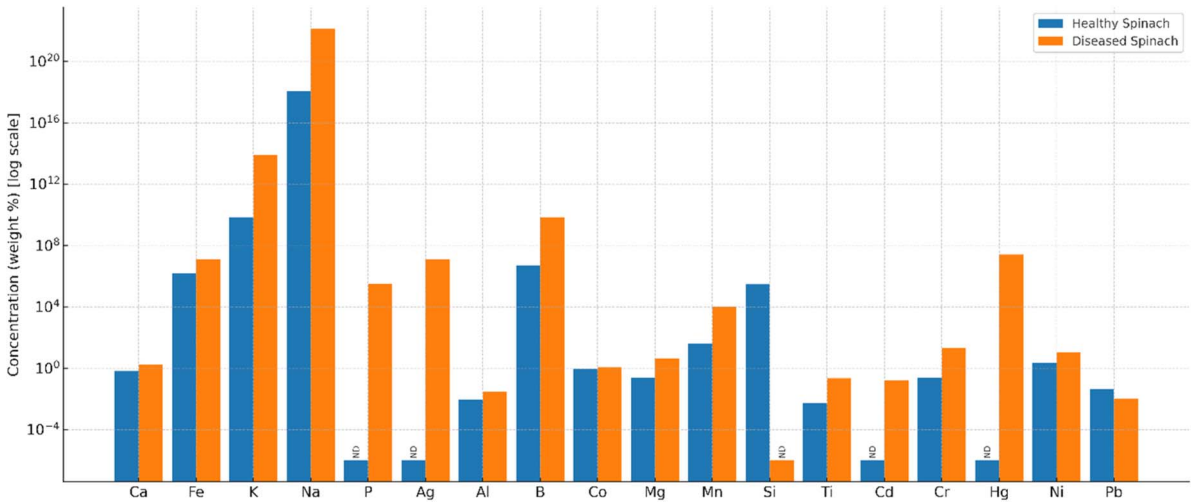

Fig. 9 Comparison of elemental concentrations (weight%, log scale) between healthy and diseased spinach (*Spinacia oleracea*) determined using IRSAC-corrected CF-LIBS.

in line with the established critical roles of these elements in spinach physiology. On the other hand, the potentially toxic elements (Cd, Cr, Ni, Pb and Hg) had low absolute concentrations but were always greater in the diseased samples than in the healthy ones, indicating stress-induced change in the elemental uptake or retention. Overall, the CF-LIBS with the IRSAC method proved to be useful in separating the healthy and diseased spinach based on the clear distinctions in the macro-, micro-, and toxic elements profiles.

3.5 Method validation: cross verification with ICP-OES

To check the quantitative reliability of the IRSAC-corrected CF-LIBS values, the elemental concentrations obtained through CF-LIBS were cross verified against independent values obtained with inductively coupled plasma-optical emission spectroscopy (ICP-OES). The validation elements to be used are Ca, Mg, K, Fe, and Mn which are nutritionally important macro and micro-nutrients present in leafy vegetables and are widely used as reference elements in LIBS validation studies.[60] A direct comparison between the ICP-OES and IRSAC-CF-LIBS measurements in the healthy and diseased spinach leaves is given in Table 3. For all selected elements, IRSAC corrected CF-LIBS values were within 7–11% deviation range with the ICP-OES standard, and this shows high quantitative convergence. This agreement also supports the quantitative consistency of the IRSAC-corrected CF-LIBS results for strongly self-absorbed elements such as K and Ca, which showed larger correction ratios but still produced CF-LIBS concentrations within 7–11% deviation relative to ICP-OES. The close correspondence implies that IRSAC is efficient in controlling self-absorption impairments and equilibrating the line-intensity ratios, enabling CF-LIBS to provide with the concentration estimates that are stable and comparable to the conventional wet-chemical techniques. This degree of correspondence is comparable to the previous CF-LIBS verifications of plant leaves and herbs where variations of 5–15% in comparison to ICP-OES or ICP-AES were mentioned.[61–63]

Table 3 Comparison of IRSAC-corrected CF-LIBS elemental concentrations with ICP-OES reference values for healthy and diseased spinach leaves

Element	ICP-OES healthy (ppm)	IRSAC-CF-LIBS healthy (ppm)	% Error (healthy)	ICP-OES diseased (ppm)	IRSAC-CF-LIBS diseased (ppm)	% Error (diseased)
Ca	8200	7610	7.2	6100	5560	8.8
Mg	2950	2720	7.8	2100	1950	7.1
K	28 500	26 480	7.1	21 300	19 580	8.1
Fe	185	170	8.1	142	131	7.7
Mn	68	61	10.3	52	48	7.6

Moreover, the concentration levels that have been obtained in this study are in the same order of magnitude with other LIBS and ICP-based nutrient analysis of spinach and other green matrices that have been reported in the past. Previous validation to date of LIBS-ICP has demonstrated that Mg, Ca, Na and other macronutrients are commonly found usually within the 10^3–10^4 ppm range in spinach leaves,[64] and that the equivalent levels of these nutrients have been observed in a wide range of plant materials with LIBS backed by the ICP-based quantification system.[65] The fact that this literature reported ranges of nutrients are consistent with the present findings only further ascertains the physical viability and analytical strength of the IRSAC-corrected CF-LIBS method to quantitative elemental profiling of spinach. Na was excluded only from the ICP-OES cross-validation shown in Table 3 because the Na response in the digested spinach matrix was saturated at the dilution used. However, Na was not excluded from the CF-LIBS mass-balance calculation. In the CF-LIBS procedure, Na remained included in the normalization sum together with all detected elements, so that $\sum C_i^{\mathrm{rel}} = 1$. Therefore, the exclusion of Na from the ICP-OES comparison did not affect the CF-LIBS normalization. The agreement between IRSAC-corrected CF-LIBS and ICP-OES for Ca, Mg, K, Fe and Mn, with deviations within 7–11%, provides an external check of the quantitative consistency of the corrected elemental profile under the present experimental conditions. Future ICP-OES validation of Na should be performed using a higher dilution or an alternative analytical line.

3.6 PCA and machine learning classification

To ensure reproducibility, the machine-learning workflow used IRSAC-corrected full LIBS spectra (190–770 nm) as input features after baseline correction and normalization. For each class (healthy/diseased), five biological samples were analyzed, and each provided 20 independent shots, giving 100 spectra per class. The 20 individual shot spectra from each pellet were retained as separate spectra and were not averaged before PCA or machine learning. IRSAC correction factors were calculated once for each pellet from the corresponding average spectrum to improve the signal-to-noise ratio for plasma-temperature and correction-factor estimation. These pellet-specific, line-dependent correction factors were then applied to each of the 20 individual shot spectra from the same pellet, thereby preserving shot-to-shot spectral variability while reducing systematic self-absorption effects. Principal Component

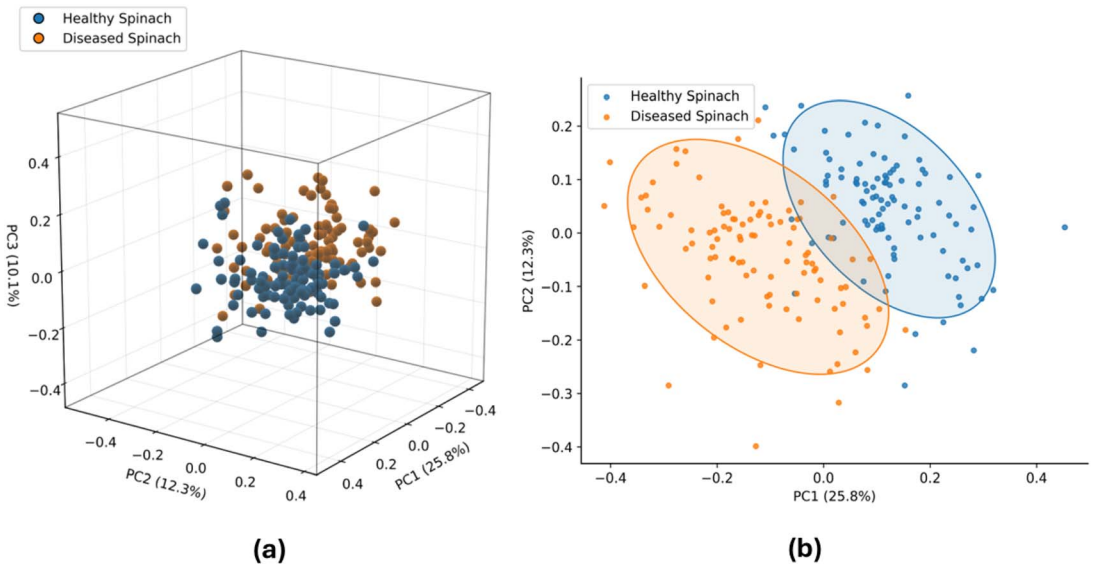

Fig. 10 (a) 3D Principal Component Analysis (PCA) plot of healthy and diseased spinach samples based on LIBS spectral data. (b) 2D PCA score plot of PC1 *vs.* PC2 with 95% confidence ellipses. Clear clustering of healthy and diseased spinach samples demonstrates separation based on elemental composition differences.

Analysis (PCA) was used to assess the potential discrimination of LIBS data of healthy and diseased spinach samples.[66] Fig. 10(a) using the first three components (PC1 = 25.8%, PC2 = 12.3%, PC3 = 10.1%) indicated that the cumulative variance was 48.2. Despite the presence of some overlap, clustering patterns of healthy and diseased samples can be observed, with systematic differences in spectral signatures of healthy and diseased samples being apparent.[67] The further separation is highlighted by the 2D projection of PC1 *vs.* PC2 given in Fig. 10(b). The presence of confidence ellipses shows that most of the healthy samples are concentrated in the positive PC1 area, whereas diseased samples are concentrated in the negative PC1 area. This means that PC1 represents the most correlated elemental variation with the health status of plants. These results indicate that LIBS spectral data when processed by PCA can be used to give a good statistical distinction between healthy and diseased spinach. This kind of separation indicates the differences in elemental composition that are caused by disease, and it proves the possibility of PCA as a dimensionality reduction and classification method of plant health monitoring.[68]

Even though PCA has given a preliminary visualization of the separation of classes, supervised machine learning was utilised to quantitatively assess the performance of classification. Discrimination of healthy and diseased spinach with IRSAC-corrected LIBS spectra was assessed using a variety of supervised machine learning models. Classifiers were decision trees, logistic regression, support vector machine (SVM), *k*-nearest neighbours (kNN), ensemble classifiers and neural networks.[32,33] Table 4 shows model performance under LOGO cross validation by its validation accuracy, test accuracy and the computational time. In the LOGO scheme, all 20 spectra from the same pellet were kept together in the same fold, so that spectra from a given pellet were never split between training and testing. This prevented shot-level data leakage and ensured that model performance reflected generalization across pellets rather than memorization of within-pellet spectral noise. The confusion matrix was used to compute classification accuracies as:

$$\text{Accuracy} = \frac{\text{TP} + \text{TN}}{\text{TP} + \text{TN} + \text{FP} + \text{FN}} \quad (15)$$

where TP, TN,FP and FN represent true positives, true negatives, false positives and false negatives. Among the tested models, SVM based classifiers proved to be the most stable and consistent at their performance. The linear SVM provided the best balance between predictive strength and computational efficiency, with 93.8% validation accuracy and 97.5% test accuracy under pellet-level LOGO cross-validation, as shown in Fig. 11(a) and 12(a). Receiver operating characteristic (ROC) analysis also affirmed that this model has discriminatory capability, whose area under curve (AUC) values were close to 1. The performance of other models was relatively lower or less stable. Quadratic and Gaussian SVMs performed well on validation accuracy (97%) however showed lower test accuracy (89.5%) that suggests overfitting. Logistic regression models showed moderate generalization (~86–87% test accuracy) whereas neural networks were mixed with the bilayered representation having high-test accuracy and low-validation stability.

Table 4 Comparative performance of machine learning classifiers for spinach LIBS spectra

Model family	Sub-model	Validation accuracy (%)	Test accuracy (%)	Computation time (s)
Tree	Coarse tree	68.8	72.5	74.29
Logistic regression	Binary GLM logistic regression	93.3	87.0	61.77
	Efficient logistic regression	90.8	86.3	51.30
SVM	Efficient linear SVM	90.3	86.5	54.36
	Linear SVM	93.8	97.5	46.07
	Quadratic SVM	97.1	89.5	118.37
	Cubic SVM	80.0	87.5	130.60
	Fine Gaussian SVM	87.0	84.5	134.66
	Medium Gaussian SVM	97.3	89.5	146.90
kNN	Fine KNN	16.3	45.0	204.24
	Medium KNN	52.5	52.5	209.11
	Coarse KNN	50.0	50.0	224.81
	Cosine KNN	94.8	87.5	229.90
	Cubic KNN	54.4	52.5	246.11
	Weighted KNN	14.4	37.5	251.70
Ensemble	Boosted trees	50.0	67.5	180.21
	Bagged trees	73.1	75.0	184.21
	Subspace discriminant	94.4	91.0	196.69
	Subspace KNN	12.5	50.0	200.64
	RUSBoosted trees	50.0	67.5	213.11
Neural network	Narrow neural net	87.1	93.0	87.54
	Medium neural net	93.8	86.0	92.76
	Wide neural net	94.1	88.0	94.49
	Bilayered neural net	84.4	97.5	99.94
	Trilayered neural net	81.9	92.5	101.60

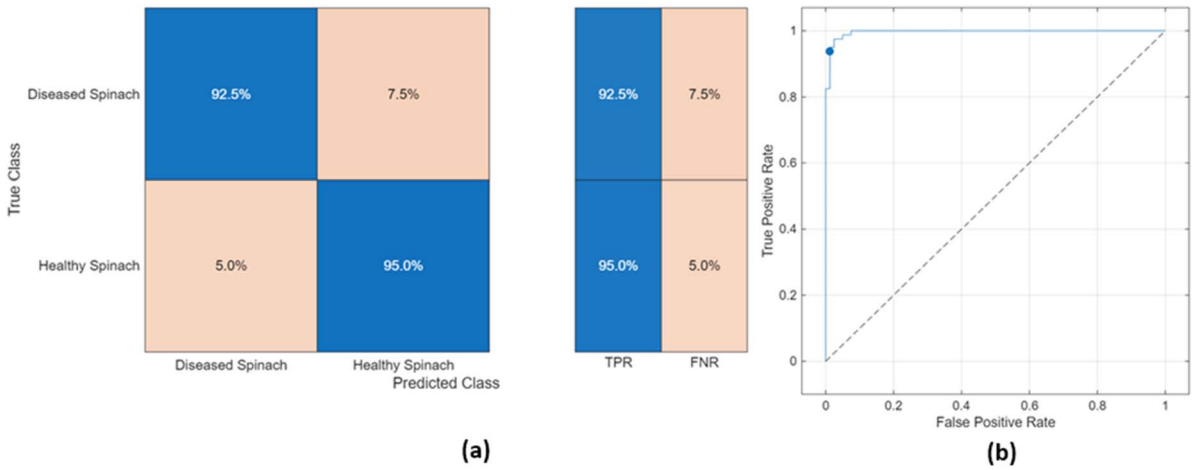

Fig. 11 Validation results of the linear SVM model for classification of healthy and diseased spinach LIBS spectra. (a) Confusion matrix shows 92.5% correct classification of diseased spinach and 95% for healthy spinach. (b) Receiver Operating Characteristic (ROC) curve with an area under the curve (AUC) approaching 1, confirming excellent discriminative ability.

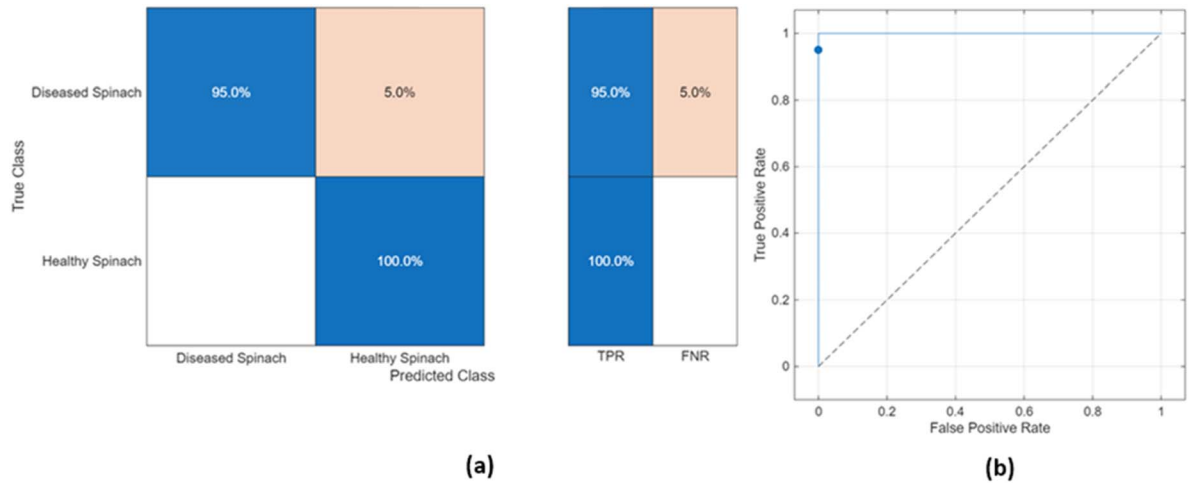

Fig. 12 Test results of the linear SVM. (a) Confusion matrix showing 95% correct classification for diseased and 100% for healthy spinach samples. (b) Receiver Operating Characteristic (ROC) curve with perfect separation (AUC = 1.0), demonstrating outstanding classification performance.

The ensemble methods yielded moderately high (~91% test) accuracy, decision trees and various kNN versions yielded low (<75%), and the decision tree and multiple kNN variants yielded lower performance than ensemble methods, indicating less relevance to high dimensional LIBS spectral classification.[69]

Although pellet-level LOGO cross-validation reduces data leakage, the present dataset includes five biological samples per class; therefore, external validation using an independently collected spinach cohort will be necessary to further confirm model generalizability.

4. Conclusion

This paper presents the effective combination of Internal Reference Self-Absorption Correction (IRSAC) and Calibration-Free Laser-Induced Breakdown Spectroscopy (CF-LIBS) and machine learning in elemental profiling and health monitoring of spinach (*Spinacia oleracea*). The IRSAC technique was effective in reducing distortions in strong emission lines to obtain more precise plasma parameters and elemental concentrations. There were evident variations in the macro, micro, and trace-element distributions in healthy and diseased samples, disease stress being linked to the repressed Ca, K, and Mg signals and high concentrations of potentially toxic elements Cd, Pb, and Hg. The plasma diagnostics established credible excitation temperatures and electron densities in LTE conditions, which forms a strong foundation on CF-LIBS quantification which was validated by ICP-OES results. Classifiers of machine learning, especially support vector machines and logistic regression, obtained accuracy more than 90%, and linear SVM obtained 97.5% test accuracy on this dataset. This shows the strength of integrating physically corrected LIBS spectra with powerful computational models to detect disease.

In general, the CF-LIBS and machine learning system developed with the help of IRSAC and presented in this paper provides a fast and potentially field-deployable once adapted to portable instrumentation and simplified sample handling. In addition to spinach, the technology has a great potential in the wider agricultural use, such as precision nutrient control, early disease diagnosis, and food safety. Future research can build upon this by applying the method to multi-crop systems, incorporating portable LIBS instrumentation, and optimizing chemometric pipelines to provide real time on-site analysis.

Conflicts of interest

There are no conflicts to declare.

Data availability

All data supporting the findings of this study will be made available as supplementary information (SI) accompanying the published article. Supplementary information: raw LIBS spectra that can be used to reproduce all the results. See DOI: https://doi.org/10.1039/d6ra01889k.

References

1 L. M. John and K. K. Anoop, A numerical procedure for understanding the self-absorption effects in laser induced breakdown spectroscopy, *RSC Adv.*, 2023, **13**(42), 29613–29624.
2 Z. Hu, F. Chen, D. Zhang, Y. Chu, W. Wang, Y. Tang and L. Guo, A method for improving the accuracy of calibration-free laser-induced breakdown spectroscopy by exploiting self-absorption, *Anal. Chim. Acta*, 2021, **1183**, 339008.
3 M. Ciopec, B. Pascu and P. Negrea, Inductively coupled plasma optical spectroscopy and atomic absorption spectroscopy, in *Microbial Electrochemical Technologies: Fundamentals and Applications*, 2023, vol. 1, pp. 201–228.
4 L. Wang, G. Tolok, Y. Fu, L. Xu, L. Li, H. Gao and Y. Zhou, Application and research progress of laser-induced breakdown spectroscopy in agricultural product inspection, *ACS Omega*, 2024, **9**(23), 24203–24218.
5 U. Sarma and B. TR, Dietary phytonutrients in common green leafy vegetables and the significant role of processing techniques on spinach: a review, *Food Prod., Process. Nutr.*, 2024, **6**(1), 10.
6 S. Hussain, Advancing plant health management: challenges, strategies, and implications for global agriculture, *International Journal of Agriculture and Sustainable Development*, 2024, **6**(2), 73–89.
7 C. Farber and D. Kurouski, Raman spectroscopy and machine learning for agricultural applications: chemometric assessment of spectroscopic signatures of plants as the essential step toward digital farming, *Front. Plant Sci.*, 2022, **13**, 887511.
8 R. Falcioni, J. V. Gonçalves, K. M. Oliveira, W. C. Antunes and M. R. Nanni, VIS-NIR-SWIR hyperspectroscopy combined with data mining and machine learning for classification of predicted chemometrics of green lettuce, *Remote Sens.*, 2022, **14**(24), 6330.
9 C. Aragón and J. A. Aguilera, Characterization of laser induced plasmas by optical emission spectroscopy: a review of experiments and methods, *Spectrochim. Acta, Part B*, 2008, **63**(9), 893–916.
10 R. Falcioni, T. Moriwaki, M. S. Gibin, A. Vollmann, M. C. Pattaro, M. E. Giacomelli, F. Sato, M. R. Nanni and W. C. Antunes, Classification and prediction by pigment content in lettuce (Lactuca sativa L.) varieties using machine learning and ATR-FTIR spectroscopy, *Plants*, 2022, **11**(24), 3413.
11 M. Z. Khan, A. A. Khan, A. A. Laghari, Z. A. Shaikh, M. A. Khani, D. M. Morkovkin, O. Gavel, S. E. Shkodinsky, S. Makar and D. E. Taburov, Comparative case study: an evaluation of performance computation between support vector machine, k-nearest neighbors, k-mean, and principal component analysis, *Tianjin Daxue Xuebao, Ziran Kexue Yu Gongcheng Jishuban*, 2022, **55**(04), 388–403.
12 I. T. Jolliffe and J. Cadima, Principal component analysis: a review and recent developments, *Philos. Trans. R. Soc. A Math. Phys. Eng. Sci.*, 2016, **374**(2065), 20150202.
13 M. Rezaei, F. Rezaei and P. Karimi, Using various machine learning algorithms for quantitative analysis in laser induced breakdown spectroscopy, *arXiv*, 2023, preprint, arXiv:2304.07786, DOI: 10.48550/arXiv.2304.07786.
14 B. Liu, L. Stein, K. Cochran, L. J. du Toit, C. Feng and J. C. Correll, Three new fungal leaf spot diseases of spinach in the United States and the evaluation of fungicide efficacy for disease management, *Plant Dis.*, 2021, **105**(2), 316–323.
15 M. Manzoor, M. Faheem, M. Nadeem, G. Shreen, F. Hayat, A. Younis and Y. Jamil, A machine learning assisted approach to classify rose species and varieties with laser induced breakdown spectroscopy, *Anal. Chim. Acta*, 2025, **28**, 344489.
16 F. N. Mikkelsted, D. Adén, T. Nikolajsen and K. H. Laursen, A novel LIBS method for quantitative and high-throughput analysis of macro-and micronutrients in plants, *J. Anal. At. Spectrom.*, 2024, **39**(8), 2008–2020.
17 H. B. Andrews, M. Z. Martin, A. M. Wymore and U. C. Kalluri, Rapid in situ nutrient element distribution in plants and soils using laser-induced breakdown spectroscopy (LIBS), *Plant Soil*, 2024, **495**(1), 3–12.
18 S. Musazzi and U. Perini, Laser-induced breakdown spectroscopy, *Springer Opt. Sci.*, 2014, **182**, E1–E2.
19 Avantes, *AvaSoft software*, 2023, https://www.avantes.com/products/software.
20 L. M. Narlagiri and V. R. Soma, Improving the signal-to-noise ratio of atomic transitions in LIBS using two-dimensional correlation analysis, *OSA Continuum*, 2021, **4**(9), 2423–2441.
21 X. Xu, G. Teng, Q. Wang, Z. Zhao, K. Wei, M. Bao, Y. Zheng and T. Luo, Spectral preprocessing combined with feature selection improve model robustness for plastics samples classification by LIBS, *Front. Environ. Sci.*, 2023, **11**, 1175392.

22 M. H. Zaman, F. Rehman, M. S. Tahir, M. Faheem and Y. Jamil, A study on the effect of preprocessing and normalization on classification of plant samples in machine learning assisted laser-induced breakdown spectroscopy, *Arabian J. Sci. Eng.*, 2024, **49**(7), 10003–10019.
23 P. H. Eilers and H. F. Boelens, Baseline correction with asymmetric least squares smoothing, in *Leiden University Medical Centre Report*, 2005, vol. 1, suppl. 1, p. 5.
24 S. M. Iqbal, Z. Uddin, Z. A. Umar, N. Ahmed, R. Ahmed and M. A. Baig, Analysis of Lakhra coal by calibration free laser-induced breakdown spectroscopy (CF-LIBS) and comparison of self-absorption correction procedures, *Anal. Lett.*, 2022, **55**(1), 11–23.
25 J. A. Aguilera and C. Aragón, Characterization of a laser-induced plasma by spatially resolved spectroscopy of neutral atom and ion emissions: comparison of local and spatially integrated measurements, *Spectrochim. Acta, Part B*, 2004, **59**(12), 1861–1876.
26 H. R. Griem, *Principles of plasma spectroscopy*, 2005.
27 R. W. McWhirter, Spectral intensities, in *Plasma diagnostic techniques*, 1965, suppl. 65, p. 201.
28 E. Tognoni, G. Cristoforetti, S. Legnaioli and V. Palleschi, Calibration-free laser-induced breakdown spectroscopy: state of the art, *Spectrochim. Acta, Part B*, 2010, **65**(1), 1–14.
29 G. Cristoforetti, A. De Giacomo, M. Dell'Aglio, S. Legnaioli, E. Tognoni, V. Palleschi and N. J. Omenetto, Local thermodynamic equilibrium in laser-induced breakdown spectroscopy: beyond the McWhirter criterion, *Spectrochim. Acta, Part B*, 2010, **65**(1), 86–95.
30 R. E. Russo, X. Mao, J. J. Gonzalez, V. Zorba and J. Yoo, Laser ablation in analytical chemistry, *Anal. Chem.*, 2013, **85**(13), 6162–6177.
31 S. Wold, K. Esbensen and P. Geladi, Principal component analysis, *Chemometr. Intell. Lab. Syst.*, 1987, **2**(1–3), 37–52.
32 L. Breiman, Random forests, *Mach. Learn.*, 2001, **45**(1), 5–32.
33 R. Kohavi, A study of cross-validation and bootstrap for accuracy estimation and model selection, *Int. Joint Conf. Artif. Intell.*, 1995, **14**(2), 1137–1145.
34 N. Lee and J. Brgoch, From Model to Material: Machine Learning Enabled Discovery of LED-Compatible Phosphors, *Adv. Opt. Mater.*, 2026, **14**(1), e02034.
35 A. Rahdar and S. Fathi-Karkan, Physics informed machine learning for predictive toxicology and optimization of curcumin nanocarriers, *Sci. Rep.*, 2026, **16**, 4172.
36 A. Savitzky and M. J. Golay, Smoothing and differentiation of data by simplified least squares procedures, *Anal. Chem.*, 1964, **36**(8), 1627–1639.
37 G. Kim, J. Kwak, J. Choi and K. Park, Detection of nutrient elements and contamination by pesticides in spinach and rice samples using laser-induced breakdown spectroscopy (LIBS), *J. Agric. Food Chem.*, 2012, **60**(3), 718–724.
38 P. Shukla, R. Kumar and A. K. Raib, Detection of minerals in green leafy vegetables using laser induced breakdown spectroscopy, *J. Appl. Spectrosc.*, 2016, **83**(5), 872–877.
39 D. Zhang, X. Niu, J. Nie, S. Shi, H. Ma and L. Guo, Plasma parameters correction method based on plasma image-spectrum fusion for matrix effect elimination in LIBS, *Opt. Express*, 2024, **32**(7), 10851–10861.
40 S. N. Thakur and J. P. Singh, Fundamentals of LIBS and recent developments, in *Laser-Induced Breakdown Spectroscopy*, 2020, pp. 3–22.
41 D. S. Ferreira, E. R. Pereira-Filho, F. M. Pereira, D. F. Andrade and R. R. Gamela, Data Fusion in LIBS Food Analysis, in *Laser-Induced Breakdown Spectroscopy in Biological, Forensic and Materials Sciences*, Springer Nature Switzerland, Cham, 2025, pp. 491–505.
42 A. De Giacomo and J. Hermann, Laser-induced plasma emission: from atomic to molecular spectra, *J. Phys. D Appl. Phys.*, 2017, **50**(18), 183002.
43 H. Griem, *Spectral line broadening by plasmas*, Elsevier, 2012.
44 N. Konjevic and W. L. Wiese, Experimental Stark widths and shifts for non-hydrogenic spectral lines of ionized atoms, *J. Phys. Chem. Ref. Data*, 1976, **5**(2), 259–308.
45 Y. Ralchenko, Atomic physics and spectroscopy during the first 50 years of JPCRD, *J. Phys. Chem. Ref. Data*, 2022, **51**(1), 013101.
46 V. Palleschi, Avoiding misunderstanding self-absorption in laser-induced breakdown spectroscopy (LIBS) analysis, *Spectroscopy*, 2022, **37**(8), 60–62.
47 A. H. Farhadian and M. Mollaei, Homogeneity analysis of medicine tablets by laser induced breakdown spectroscopy combined with multivariate methods, *Eur. J. Pharm. Biopharm.*, 2024, **205**, 114579.
48 Y. Yang, X. Hao and L. Ren, Correction of self-absorption effect in calibration-free laser-induced breakdown spectroscopy (CF-LIBS) by considering plasma temperature and electron density, *Optik*, 2020, **208**, 163702.
49 D. M. Diaz Pace and M. J. Molina, τ-Algorithm for gathering spectroscopic information by modeling emission line shapes: application to laser-induced plasmas, *J. Opt. Soc. Am. B*, 2023, **40**(4), C1–C7.
50 M. J. Molina, C. Aragón, J. A. Aguilera, C. Costa-Vera and D. M. Díaz Pace, Improving Quantitative Analysis of Lithium in Brines Using Laser-Induced Breakdown Spectroscopy with τ-Algorithm (τLIBS), *Atoms*, 2025, **13**(11), 90.
51 L. Sun and H. Yu, Correction of self-absorption effect in calibration-free laser-induced breakdown spectroscopy by an internal reference method, *Talanta*, 2009, **79**(2), 388–395.
52 J. Hou, L. Zhang, W. Yin, S. Yao, Y. Zhao, W. Ma, L. Dong, L. Xiao and S. Jia, Development and performance evaluation of self-absorption-free laser-induced breakdown spectroscopy for directly capturing optically thin spectral line and realizing accurate chemical composition measurements, *Opt. Express*, 2017, **25**(19), 23024–23034.
53 V. K. Singh, N. Sharma, O. N. Verma, V. K. Singh, D. K. Tripathi, Y. Lee, S. Kumar, P. K. Rai and M. A. Gondal, Application of LIBS to elemental analysis and mapping of plant samples, *At. Spectrosc.*, 2021, **42**(1), 446–453.
54 D. Bulajic, M. Corsi, G. Cristoforetti, S. Legnaioli, V. Palleschi, A. Salvetti and E. Tognoni, A procedure for correcting self-absorption in calibration free-laser induced

breakdown spectroscopy, *Spectrochim. Acta, Part B*, 2002, **57**(2), 339–353.

55 T. Ou, N. Zhang, R. Lin, N. Zhao, L. Guo, J. Li, X. Li and Q. Zhangb, Accuracy Improvement for Minor Elements Determination Using Modified Self-absorption Correction and One-point Calibration Laser-induced Breakdown Spectroscopy, *Space Explor.*, 2024, **5**, 7.

56 L. M. John, B. BN and K. K. Anoop, Continuum removal and self-absorption correction in calibration-free laser-induced breakdown spectroscopy for efficient elemental analysis, *IOP Conf. Ser. Mater. Sci. Eng.*, 2022, **1221**(1), 012020.

57 I. Rehan, M. A. Gondal, R. K. Aldakheel, M. A. Almessiere, K. Rehan, S. Khan, S. Sultana and M. Z. Khan, Determination of nutritional and toxic metals in black tea leaves using calibration free LIBS and ICP: AES technique, *Arabian J. Sci. Eng.*, 2022, **47**(6), 7531–7539.

58 M. A. Baig, R. Ahmed and Z. A. Umar, Comparison of LIBS with other analytical techniques, in *Laser induced breakdown spectroscopy (LIBS) concepts, instrumentation, data analysis and applications*, 2023, vol. 1, pp. 461–486.

59 T. A. Alrebdi, A. Fayyaz, H. Asghar, A. Zaman, M. Asghar, F. H. Alkallas, A. Hussain, J. Iqbal and W. Khan, Quantification of aluminum gallium arsenide (AlGaAs) wafer plasma using calibration-free laser-induced breakdown spectroscopy (CF-LIBS), *Molecules*, 2022, **27**(12), 3754.

60 Q. Abbass, N. Ahmed, R. Ahmed and M. A. Baig, A comparative study of calibration free methods for the elemental analysis by laser induced breakdown spectroscopy, *Plasma Chem. Plasma Process.*, 2016, **36**(5), 1287–1299.

61 L. Wang, Y. Cheng, I. M. Meftaul, F. Luo, M. A. Kabir, R. Doyle, Z. Lin and R. Naidu, Advancing soil health: challenges and opportunities in integrating digital imaging, spectroscopy, and machine learning for bioindicator analysis, *Anal. Chem.*, 2024, **96**(20), 8109–8123.

62 B. Lanza, *Development of optical measurement methodologies for in-field estimation of plant health and agricultural yield*, 2025.

63 Z. A. Umar, U. Liaqat, R. Ahmed, R. Hedwig, M. Ramli, M. A. Marpaung, K. H. Kurniawan, M. Pardede and M. A. Baig, Determination of micronutrients and toxic elements in Moringa oleifera leaves by calibration free laser-induced breakdown spectroscopy (LIBS), *Anal. Lett.*, 2022, **55**(5), 755–769.

64 L. C. Trevizan, Jr D. Santos, R. E. Samad, Jr N. D. Vieira, C. S. Nomura, L. C. Nunes, I. A. Rufini and F. J. Krug, Evaluation of laser induced breakdown spectroscopy for the determination of macronutrients in plant materials, *Spectrochim. Acta, Part B*, 2008, **63**(10), 1151–1158.

65 J. Iqbal, H. Asghar, S. K. Shah, M. Naeem, S. A. Abbasi and R. Ali, Elemental analysis of sage (herb) using calibration-free laser-induced breakdown spectroscopy, *Appl. Opt.*, 2020, **59**(16), 4927–4932.

66 R. K. Aldakheel, M. A. Gondal, M. M. Nasr, M. A. Almessiere and N. Idris, Spectral analysis of Miracle Moringa tree leaves using X-ray photoelectron, laser induced breakdown and inductively coupled plasma-optical emission spectroscopic techniques, *Talanta*, 2020, **217**, 121062.

67 Y. Wu, B. Wu, Y. Ma, M. Wang, Q. Feng and Z. He, Rapid Discrimination of Organic and Non-Organic Leafy Vegetables (Water Spinach, Amaranth, Lettuce, and Pakchoi) Using VIS-NIR Spectroscopy, Selective Wavelengths, and Linear Discriminant Analysis, *Appl. Sci.*, 2023, **13**(21), 11830.

68 N. H. Hasbi, A. Bade, F. P. Chee and M. I. Rumaling, Pattern recognition for human diseases classification in spectral analysis, *Computation*, 2022, **10**(6), 96.

69 S. Roy, R. Ray, S. R. Dash and M. K. Giri, Plant disease detection using machine learning tools with an overview on dimensionality reduction, in *Data analytics in bioinformatics: a machine learning perspective*, 2021, pp. 109–144.